Modifications of some physical properties of nanostructured indium doped Co_3O_4 thin films

O. A. Chichan[a], F. H. Jasim[b], Z. M. Shaban[b,*], K. N. Hussein[c],S. S. Chiad[b], N. F. Habubi[d], Y. H. Kadhim[e], M. Jadan[f,g]
[a]*Department of Physics, College of Education for Pure Sciences, University of Babylon, Iraq*
[b]*Department of Physics, College of Education, Mustansiriyah University, Iraq*
[c]*Department of Radiology, Al-Manara College for Medical Science, Iraq*
[d] *Department of Radiology and Sonar Techniques, Alnukhba University College, Baghdad 10013, Iraq*
[e]*Department of Optics Techniques, College of Haelth and Medical Techniques, AL-Mustaqbal University, Babylon, Hillah, 51001, Iraq*
[f]*Department of Physics, College of Science, Imam Abdulrahman Bin Faisal University, P.O. Box 1982, 31441 Dammam, Saudi Arabia*
[g]*Basic and Applied Scientific Research Center, Imam Abdulrahman Bin Faisal University, P.O. Box 1982, 31441 Dammam, Saudi Arabia*

Using the chemical spray pyrolysis (CSP) technique, nanostructured undoped and Co_3O_4:In thin films are deposited. The effect of indium doping content in Cobalt ranged from 1% to 3% on optical, structural, and topographical properties of Co_3O_4 nanostructured thin films. No new peaks belonging to the In phase were seen, according to X-ray diffraction research, which revealed that pure and Co_3O_4: In thin films are polycrystalline in and cubic phase with (111), (311), (400), and (511) preferable orientation for all filmsThe Scherrer formula computation of average crystallite size shows that the size of Nano crystallites grows when doping is enhanced. AFM micrographs demonstrated how the surface shape of the films was discovered to be influenced by the inclusion of indium in the Co_3O_4 location.SEM images of Undoped Co_3O_4 and Co_3O_4:In films (CSP technique), showing separate semi-spherical blocks (120-200 nm) of nanoparticles (<30 nm). Band gap values for pure and doped were 2.52 to 2.38 eV. Resistance increases with increases Indium-doping, indicating more charge carriers and potential surface roughness influence. Sensitivity decreases with higher Indium concentrations, attributing to enhanced crystallinity and nano-crystalline size.

(Received June 16, 2024; Accepted September 18, 2024)

Keywords: Co_3O_4, Iindium doped, Spray pyrolysis technique, Structural, AFM, SEM, Optical properties, Band gap, Sensitivity

1. Introduction

Cobalt oxide is a significant transition oxide, with a great deal of attention in several sectors. It is a semiconducting material having a p-type cubic spinel structure with optical band gaps of 1.44–2.06 eV. Co_3O_4 phase was extensively studied last year due to its chemical stability and potential as a promising material. Co_3O_4 is an antiferromagnetic material with a regular spinel structure[1-4]. The cubic rock-salt structure is how cobalt monoxide crystallises [5-7]. Whereas Co_3O_4 crystallises in the typical spinel form [8-10], the opposite is true. In this structure, Co^{2+} and Co^{3+} ions are found in the interstitial tetrahedral and octahedral sites, respectively [4]. A practical and promising method to enhance the Co_3O_4 materials is doping with transparent metals like, In, Ga, and Al. [5]. Co_3O_4 thin films are made using a variety of processes RF magnetron sputtering [11], chemical vapor deposition [12], sol-gel procedure [13], ALD co-precipitation method [14],

* Corresponding author: zinam.shaban@uomustansiriyah.edu.iq
https://doi.org/10.15251/DJNB.2024.193.1319

(Atomic Layer Deposition) [15], CBD (Chemical Bath Deposition) [16], chemical spray pyrolysis (CSP) [17] and PLD (Pulsed Laser Deposition) [18], The CSP technique has a privileged , including low cost, adaptability, simplicity of usage for large deposition regions, and the ability to produce nanostructured thin films. [18]. In this research, the impact of Indium content on the physical properties of Co_3O_4 films was examined.

2. Experimental

Cobalt oxide and cobalt oxide doped with nickel (Co_3O_4) Using glass slide substrates, thin films were created using CSP process. To deposit Co_3O_4 thin, a 0.1 M cobalt chloride aqueous solution was employed as the matrix solution. To get 1% and 3% indium, 0.1 M of indium chloride ($InCl_2.6H_2O$) was used as the doping material. The substrate was heated up before the matrix solution was applied. After several tests, the following optimisation criteria were considered: A consistent substrate temperature of 400 ºC was maintained throughout the deposition process: 30 cm separated the nozzle from the substrate. The flow rate was 5 mL/min to prevent duplicate substrate cooling, and the spraying rate was 8 s, followed by 90 s. As a carrier gas, it was employed. The structural characteristics of thin films were measured using high-resolution X-ray technology operating a D8 Advance Bruker, CuKa (0.154056 nm). Surface topography was introduced using the AFM and the computerised tools Nanoscop and Dimension 3100. Surface morphology was examined by the Hitachi S-4300 scaning electron microscopy (SEM). We recorded the transmittance spectra via a double-beam UV-Vis spectrophotometer. Co_3O_4 gas sensor made with aluminum electrodes. Gas sensitivity evaluated by resistance change. Tested in cylindrical chamber.

3. Results and discussions

XRD patterns of entended films produced at 400°C is shown in Figure 1. The polycrystalline character of the produced films is confirmed by the fact that all the in-doped Co_3O_4 has the same XRD peaks, such as (111), (311), (400), and (511) and that the peak location is identical to that of the pure Co_3O_4 , this behavior agree with [19-21]. As shown in Fig. 1, all films are orientated along the (111) plane, located at $2\theta = 19.08°$. The pattern in Fig. 1 clearly shows that indium dopant ions were substituted adequately into the host lattice. The detected peaks support Co_3O_4's spinel cubic nanostructure [22, 23]. All observed peaks lined up with the Co_3O_4 standard JCPDS card No. data (42-1676). The XRD analysis further validates the generation of samples with lower levels of contaminants. All of the In-doped Co_3O_4 retains the spinel cubic structure. The structural characteristics of the intended films are displayed in Table 1.

Size of the typical crystallite (*D*) as determined by Scherrer's formula [24, 25]:

$$D = \frac{0.9\,\lambda}{\beta cos\theta} \tag{1}$$

where β is FWHM, and θ is Bragg angle. It is observed that the correct integration of In^{3+} ions into the Co^{3+}ionic sites causes the predicted nanocrystallite size to grow with an increase in indium concentration. (311) plane is seen for the lowest Indium concentration level (0.01M), which can be attributed to small crystal size [26, 27], and pronounced weak crystallisation was also seen. Peak intensities rise with increasing doping levels, indicating enhanced crystallisation. [28-29]. The greater size of the In^{3+} ions (0.080 nm) replaced by the smaller Co^{3+}ionic (0.074 nm) sites causes the peak location of the (111) plane to be somewhat displaced to a lower angle side, as shown in the XRD pattern, which agrees with [30,31]. The promising 0.03M substitution of a doping element into the host matrix has an impact on the crystallite size. The greater value of dislocation density verifies the earlier discovery [32, 33] and is related to the restriction defects placed on crystallite formation. As the amount of indium doping was increased, the crystallite size rose as well.

The formula may be used to get the microstrain (δ) values of Co_3O_4 thin films. [34, 35]:

$$\varepsilon = \frac{\beta cos\theta}{4} \tag{2}$$

When the microstrain was examined, the highest value for the undoped Co_3O_4 was around 22.35 x10^4. The minimal value, achieved at a concentration of 0.03 indium doped Co_3O_4, was 19.89 x 10^4, while the value obtained at a concentration of 0.01 indium was 20.69 104. The increase in strain in the film may cause a smaller average particle size, and similar effects of particle size reduction with strain increase have been shown [36-37].

The dislocation density (δ) is determined using the formula as the dimension of dislocation per unit volume associated with the density of flaws in the sample. [38, 39]:

$$\delta = \frac{1}{D^2} \tag{3}$$

Analysis of the dislocation density reveals that pure Co_3O_4 has a dislocation density of 41.56 x10^{14}. The dislocation density changes when a dopant is added. As a result, doping indium onto Co_3O_4 will undoubtedly cause the dislocation density to change. δvalue is determined to be 20.691014 at 0.01 indium concentration. The lowest δ observed in the films is around 32.841014 for 0.03 indium concentration, which implies a reduction in defects and an improvement in crystalline quality. This is consistent with previously written works [40, 41]. The (δ) changed with doping, as seen in Fig. 2.

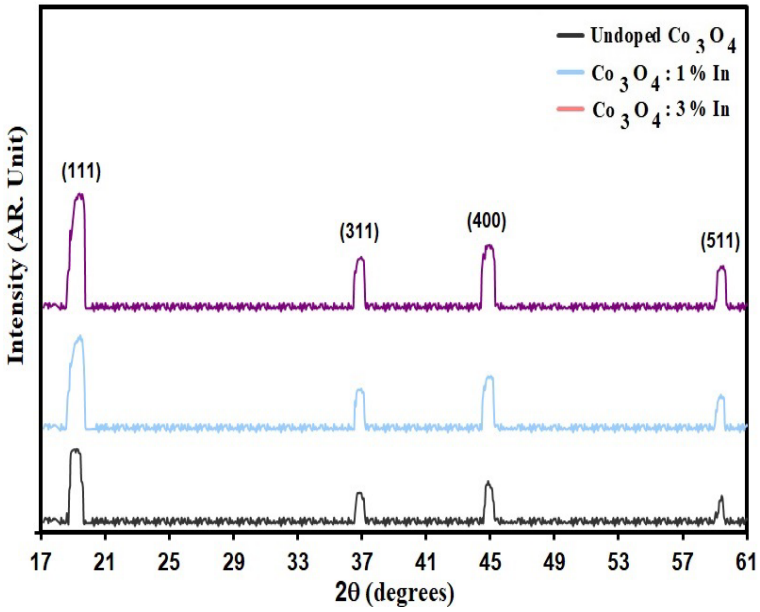

Fig. 1. XRD patterns of intended films.

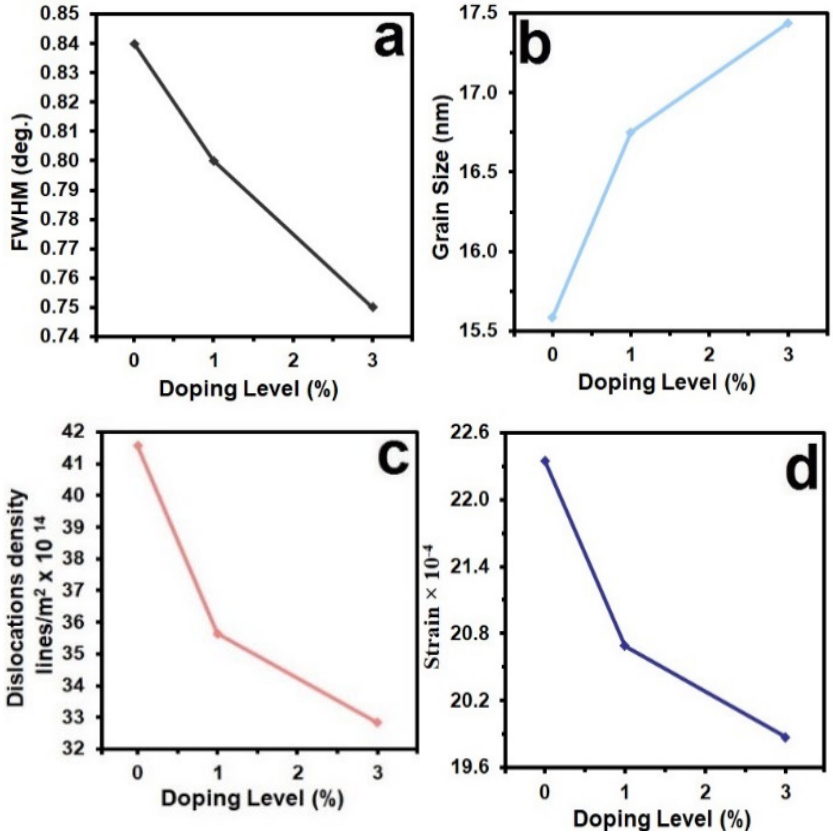

Fig. 2. X-ray parameter of pure and Co_3O_4: In films.

Table 1. Microstructural parameters of pure and Co_3O_4: In films.

Specimen	2 θ (°)	(hkl) Plane	FWHM (°)	E_{g1} (eV)	E_{g2} (eV)	D (nm)	Dislocations density ($\times 10^{14}$) (lines/m^2)	Strain ($\times 10^{-4}$)
Undoped Co_3O_4	19.08	111	0.84	1.54	2.52	15.58	41.56	22.35
Co_3O_4: 1% In	19.05	111	0.80	151	2.46	16.75	35.64	20.69
Co_3O_4: 3% In	19.01	111	0.75	1.47	2.38	17.44	32.84	19.89

AFM measurements of particle size P_{av} are much greater than XRD measurements. The indium content affects the Co_3O_4 roughness (RMS) in thin films. Table 2 provides the films' average roughness (Ra) and root mean square (RMS) values. Notably, as indium doping increases, the roughness of film surfaces diminishes. The inclusion of indium may have raised the size of the crystallites, which has raised the roughness. Because of the samples' enhanced active surface area, as a result, super-capacitor applications find them to be appealing materials [11, 42]. The surface roughness of indium addition falls from 8.76 nm to 3.45 nm with higher doping of Co_3O_4 films at 3%.

Table 2. AFM parameters of the intended films.

Samples	P_{av} nm	R_a (nm)	RMS (nm)
Undoped Co_3O_4	73.6	8.76	9.66
Co_3O_4: 1% In	36.1	6.03	8.45
Co_3O_4: 3% In	27.5	3.45	2.23

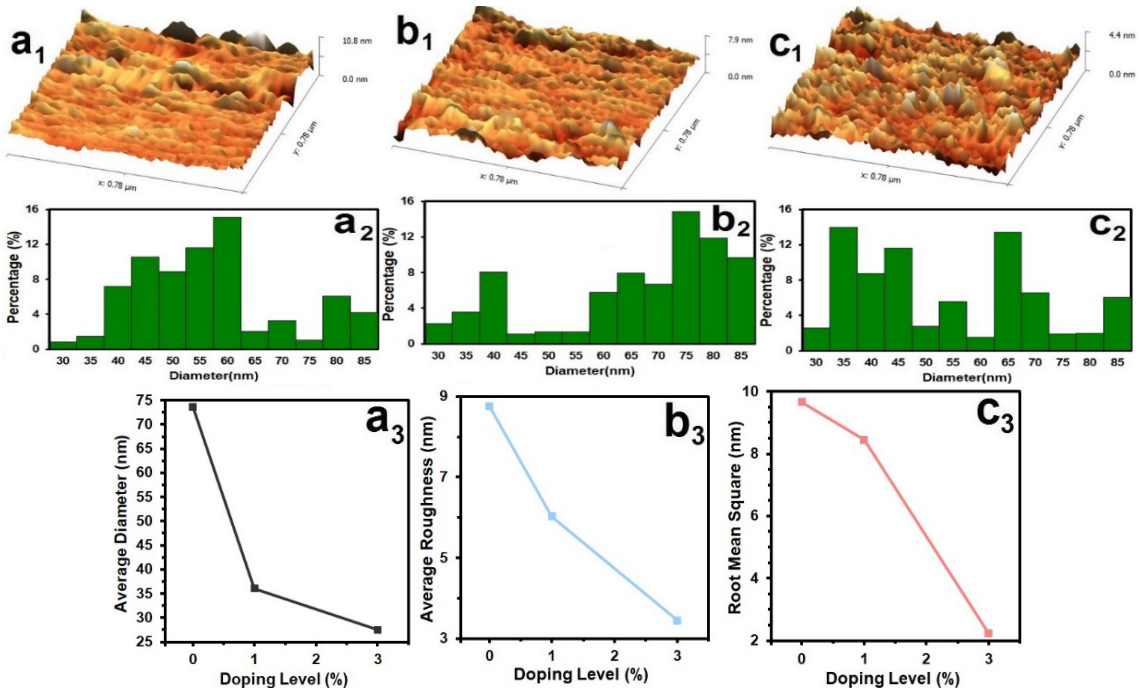

Fig. 3. AFM information of grown films.

Figure 4 illustrates SEM images of the Co_3O_4 and Co_3O_4:In films, fabricated through the chemical spray pyrolysis (CSP) technique. The SEM images provide insight into morphology and film structure, revealing the presence of well-defined semi-spherical comprising smaller nanoparticles with an average grain sixe of (38.9 , 41.5 and 55.6) nm and for udoped ,1%, and 3% indium respectively. Structural arrangement may impact the films' properties, suggesting potential applications in various fields, such as catalysis or sensing [43].

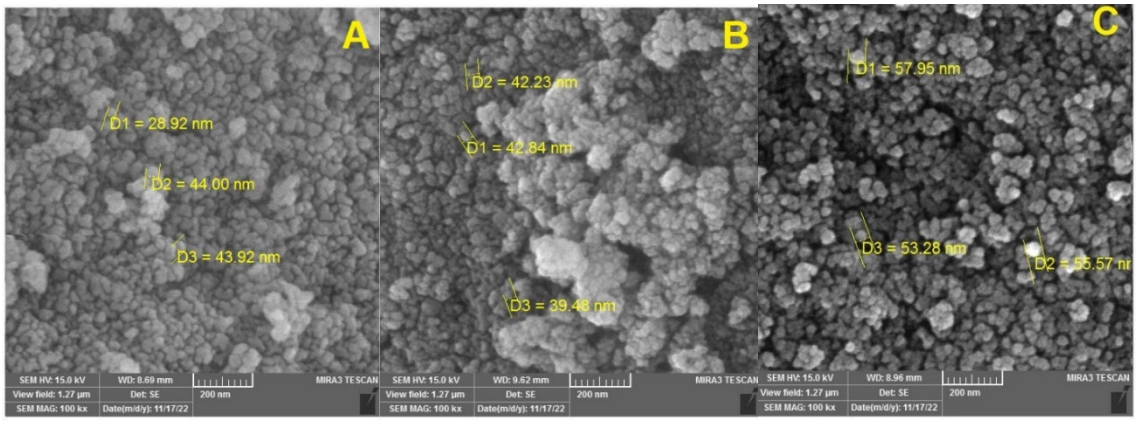

Fig.4 . SEM images of Co_3O_4 thin films with various Indium concentrations (A- Undoped Co_3O_4, B- Co_3O_4:2% In, C- Co_3O_4: 4% In).

First, UV-Vis spectra of the intended films were collected to get extensive information on the optical characteristics of films. In Fig. (5), the transmission measurement might be displayed. the Co_3O_4 and Co_3O_4:In optical transmission spectra's relationship to incident wavelength variation thin film. It is evident that for all thin films, the optical transmittance increased in the visible area

while decreasing in the UV region. The transmittance spectra gradually reduced due to the loading of indium concentration, and the band edge was changed to point toward the longer wavelength side. This edge band red shift indicates the band gap of Co_3O_4 [44, 45].

The reported absorbance (A) and transmittance (T) are linked by [46, 47]:

$$A = \log\left(\frac{1}{T}\right) = \left(\frac{I}{I_o}\right) \tag{4}$$

where (I) is the transmitted light and (I_o) is the incident light. The transition and absorption spectra of thin films of in-doped Co_3O_4 are shown in Fig. (6). The transition absorbance values drop with increasing indium inclusion. We may infer that indium doping made Co_3O_4 films optically denser since transition level measures optical density. According to several researcher in the literature [13, 48], The transition from valence band to the band, a sub-band made by Co^{3+} ions and situated beneath the conduction band, concurs with those of previous research papers in the literature. [49].

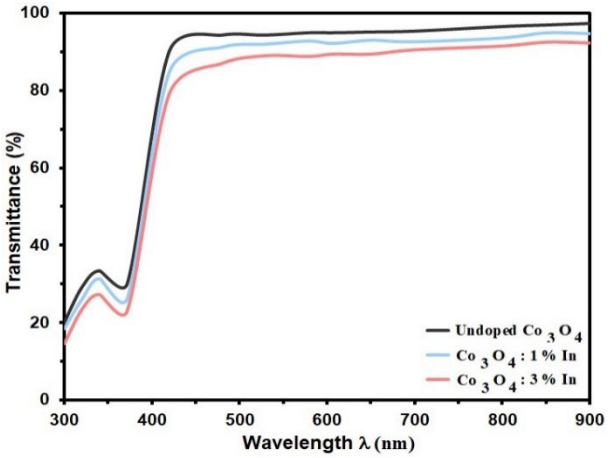

Fig. 5. T of intended films.

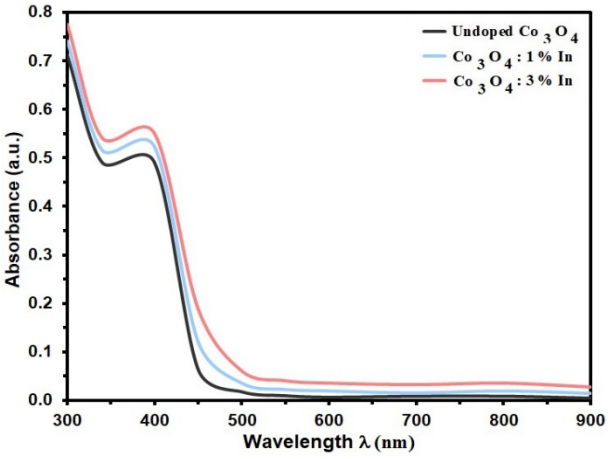

Fig. 6. Absorbance of the intended films.

The following expression was used to analyse the absorption coefficient (α). [50, 51]:

$$\alpha = \frac{(lnT^{-1})}{t} \tag{5}$$

where (**t**) is film thickness. Figure (6) depicts the relationship between (α) and wavelength (hv), the value of α >10^4 cm^{-1}. This suggests a direct transition. Fig. (7) displays the doped value of (α). The absorbance rises as indium doping increases.

The materials' prohibited band gap energy (Eg) was ascertained using the Tauc relation [52, 53].

$$\alpha h\nu = B(h\nu - E_g)^r \tag{6}$$

where, $h\nu$ is the photon energy, r = 2 for allowed direct transition, and B is a constant. As shown in Fig. (8), E_g for both undoped and In-doped films were 2.52-2.38 eV. E_g energies shift for undoped and In-doped Co_3O_4 films. According to Fig. 7, the increase in In contribution caused the Eg values to decline significantly.

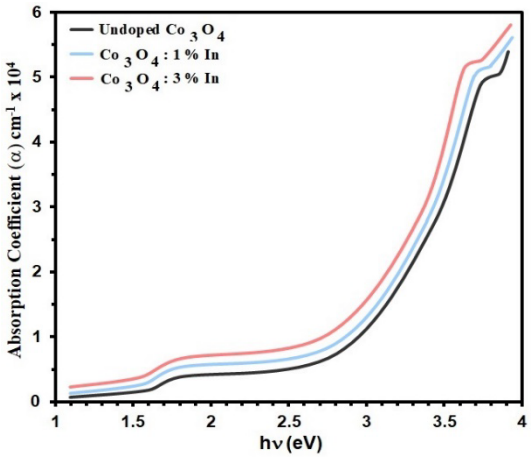

Fig. 7. α Vs hv of the grown films.

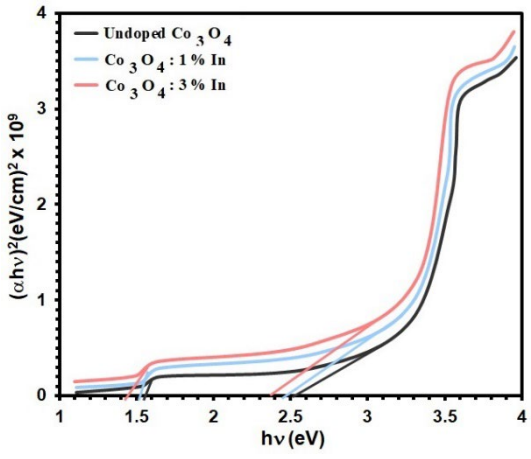

Fig. 8. $(\alpha h\nu)^2$ *Vs hv of the grown films.*

Using the relation below [54], the refractive index (n) can be calculated from the reflectance (R) data:

$$R = \frac{(n-1)^2}{(n+1)^2} \tag{7}$$

Figure 8 plots n versus wavelength for pure and Co_3O_4: In thin films with (1 and 3) % doping. n could range from about 2.80 to 2.91 at 350nm in Figure 6, which gives n plot with wavelength. These values allow the intended films to be used as antireflecting material [15, 55]. Fig. (9) also shows that n decreased with increased doping concentration though nonsequentially. The variation of n refers to modifying the ions' polarizability and the material's local field [17].

The extinction coefficient (k) can be found from Eq. 8 [56.57]:

$$k = \frac{\alpha\lambda}{4\pi} \tag{8}$$

Fig. (10) displays the fluctuations of the (k) values. The value of (k) at 390 nm for undoped film is 0.53 while for doped films at the same wavelength, equal 0.47; this difference in (k) value becomes less at the NIR region. [58, 59].

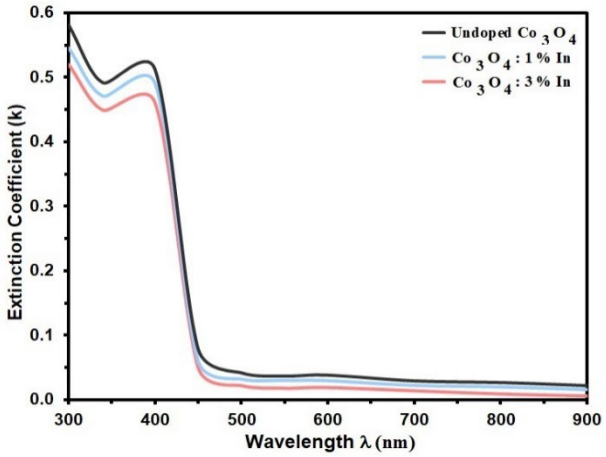

Fig. 9. n of the intended films.

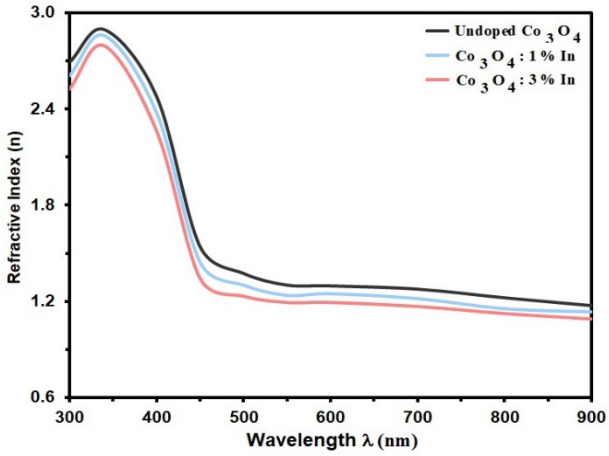

Fig. 10. k of the intended films.

Fig. (11) displays the time-dependent dynamic resistance change in response to NO_2 gas concentration (240 ppm) at an operating temperature of 150°C. The resistance values, ranging from 70.8 to 76.7 kΩ·m, exhibit an upward trend with increased doping ratios. This rise in resistance is associated with a higher number of charge carriers, potentially influenced by surface roughness. The findings suggest that the doping process affects the material's electrical properties,

making it essential to consider charge carrier concentration and surface characteristics in gas sensing applications [12].

A film's sensitivity (S) is commonly assessed by the percentage change in resistance during gas exposure, calculated as the ratio of its resistance in air (R_a)to the steady-state value (R_g) in the presence of gas. The sensor's response or detection sensitivity can be expressed as [60, 61]:

$$Sensitivity = \frac{\Delta R}{R_a} = \left|\frac{R_a - R_g}{R_a}\right| \times 100\% \quad (9)$$

Fig. (12) demonstrates the sensitivity of Co_3O_4 films, both pure and Indium-doped, to NO_2 exposure. Sensitivity decreases with higher Indium concentrations, declining from 58.8% to 24.4% (80 ppm), 63.8% to 9.8% (160 ppm), and 68.8% to 33.6% (240 ppm). The observed decrease in sensitivity of Co_3O_4 films, whether pure or Indium-doped, with higher Indium concentrations (80 ppm, 160 ppm, and 240 ppm) can be attributed to enhanced crystallinity and/or nano-crystalline size. This enhancement increases the gas reaction area and maintains a homogeneous surface. Additionally, the heightened conductivity is a result of increased carrier concentration [62, 63]. The trend in Fig. (12) suggests that sensitivity rises with the increase in gas concentration from 80 to 240 ppm. These findings emphasize the influence of dopant concentration on the gas-sensing properties [64].

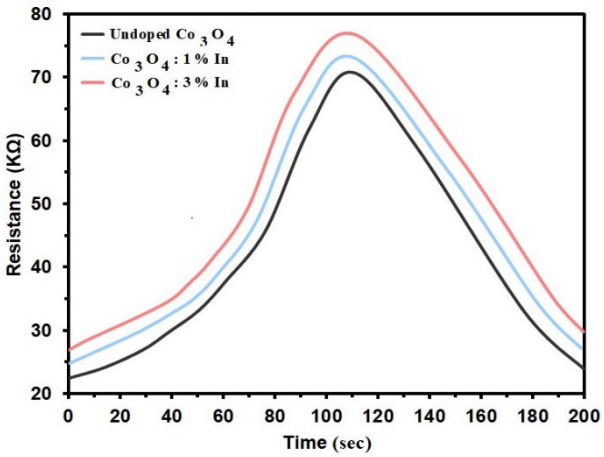

Fig. 11. displays the time-dependent resistance change of Co_3O_4:In films in response to NO_2 gas at an operating temperature of 150°C.

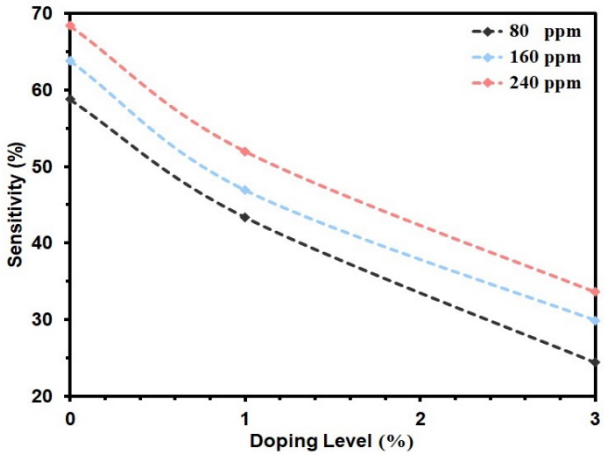

Fig. 12. Sensitivity (S) variation in Co_3O_4 thin films with different Indium concentrations.

4. Conclusion

The subject of the current investigation is the influence of indium inclusion on a few physical characteristics of Co_3O_4 nanostructure thin films generated by CSP technology. The analysis of the films' structural characteristics revealed that they feature crystalline nanostructures consistent with Co_3O_4 cubic structure. The improvement in peak intensities following the introduction of indium suggests that the films' levels of crystallisation have improved. Adding indium reduces the surface roughness values of the films, and the surface distribution of the films is essentially uniform. SEM images display Co_3O_4 and Co_3O_4:In films from CSP, showing well-defined semi-spherical nanoparticles of size range (38.9-55.6)nm. The optical property experiments demonstrated the superiority of indium-doped films as absorber layers in solar cells and that the n inclusion lowers the absorbance values of the films. The band gap values of the films were found in the range of 2.52-2.38 eV. The resistance increases with higher Indium doping, suggesting an increase in the number of charge carriers and potential influence from surface roughness. Sensitivity declines with increased Indium concentrations due to enhanced crystallinity and nano-crystalline size.

Acknowledgements

Mustansiriyah University and Alnukhba University College support this project.

References

[1] H. Jia et al.. International Journal of Hydrogen Energy, 43 (43), 19939 (2018); https://doi.org/10.1016/j.ijhydene.2018.09.036
[2] Ö. Şahin et al.. Journal of the Energy Institute, 89 (2), 182 (2016); https://doi.org/10.1016/j.joei.2015.02.005
[3] L. Wei et al. International Journal of Hydrogen Energy, 43 (3), 1529 (2018); https://doi.org/10.1016/j.ijhydene.2017.11.113
[4] S. K. Muhammad, M. O. Dawood, N. Y. Ahmed, E. S. Hassan, N. F. Habubi, S. S. Chiad, Journal of Physics: Conference Series, 1660 (1), 012057 (2020); https://doi.org/ 10.1088/1742-6596/1660/1/012057
[5] S. Akbayrak et al.. ACS Sustainable Chemistry & Engineering, 8 (10), 4216 (2020); https://doi.org/10.1021/acssuschemeng.9b07402
[6] C. Saka et al.. International Journal of Hydrogen Energy 45 (30), 15086 (2020); https://doi.org/10.1016/j.ijhydene.2020.03.238
[7] D. G. Tong. RSC Advances, 10 (21), 12354 (2020); https://doi.org/10.1039/D0RA90028A
[8] S. S. Chiad, K. H. Abass, T. H. Mubarak, N. F. Habubi, M. K. Mohammed, A. A. , Khadayeir, Journal of Global Pharma Technolog, 11(4), 369-375 (2019).
[9] J. Guo et al.. Applied Catalysis B: Environmental, 265, (2020); https://doi.org/10.1016/j.apcatb.2019.118584
[10] F. Zhong et al.. International Journal of Hydrogen Energy, 43 (49), 22273 (2018); https://doi.org/10.1016/j.ijhydene.2018.10.064
[11] C. L. Liao, Y. H. Lee, S. T. Chang, K. Z. Fuang, J. Pow. Sour.. 158, 1379 (2006); https://doi.org/10.1016/j.jpowsour.2005.10.014
[12] Z. S. Mehrabadi, A. Ahmadpour, N .Shahtahmasebi, M. M. B. Mohagheghi, Physics Scripta, 84, (1-4) (2011); https://doi.org/10.1088/0031-8949/84/01/015801
[13] F. Svegl, B. Orel, I.G. Svegl, V. Kaucic, Electr. Acta, 45, 4359 (2000); https://doi.org/10.1016/j.electacta.2006.02.028
[14] Pal J., Chauhan P., Mat. Charact., 61, 575 (2010); https://doi.org/10.1039/c3dt52391h

[15] K. B. Klepper, O. Nilson, H. Fjellvag, J. Cryst. Grow., 307, 457 (2006); https://doi.org/10.1039/c3dt52391h
[16] Z. W. Fu, Y. Wang, Y. Zhang, Q. Z. Qin, Sol. St. Ionics, 170, 105 (2004); https://doi.org/10.1002/adma.202313532
[17] L. D. Kadam, S. H. Pawar, P. S. Patil, Mat. Chem. Phy., 68, 280 (2001). https://doi.org/10.1016/S0927-0248(00)00404-9
[18] S.-L. Chou, J. Z. Wang, H. K. Liu, S. H. Dou, J. Pow. Sour, 182, 359 (2008); https://doi.org/10.1016/j.electacta.2016.12.121
[18] F. Wang et al., International Journal of Hydrogen Energy, 44 (26), 13185 (2019); https://doi.org/10.1016/j.ijhydene.2019.01.123
[19] B. Coşkuner Filiz et al., International Journal of Hydrogen Energy, 44 (53), 28471 (2019); https://doi.org/10.1016/j.ijhydene.2019.01.038
[20] C. Xu et al., Journal of Materials Chemistry, A 6 (29), 14380 (2018); https://doi.org/10.1039/C8TA03572E
[21] Y. Tonbul et al., J. Colloid Interface Sci, 553, 581 (2019); https://doi.org/10.1016/j.jcis.2019.06.038
[22] A. S. Alkelaby, K. H. Abass, T. H. Mubarak, N. F. , Habubi, S. S. Chiad, I. Al-Baidhany, Journal of Global Pharma Technology 11(4), 347-352 (2019).
[23] N. Y. Ahmed, B. A. Bader, M. Y. Slewa, N. F. Habubi, S. S. Chiad, NeuroQuantology, 18(6), 55-60 (2020); https://doi.org/10.1016/j.jlumin.2021.118221
[24] A. A. Khadayeir, K. H. Abass, S. S. Chiad, M. K. Mohammed, N. F. Habubi, T. K. Hameed, I. A. Al-Baidhany, Journal of Engineering and Applied Sciences, 13 (22), 9689-9692 (2018).
[25] Khadayeir, A. A., Hassan, E. S., Mubarak, T. H., Chiad, S.S., Habubi, N. F., Dawood, M.O., Al-Baidhany, I. A., Journal of Physics: Conference Series, 1294 (2) 022009(2019); https://doi.1088/1742-6596/1294/2/022009
[26] A. J. Ghazai, O. M. Abdulmunem, K. Y. Qader, S. S. Chiad, N. F. Habubi, AIP Conference Proceedings 2213 (1), 020101 (2020); https://doi.org/10.1063/5.0000158
[27] H. A. Hussin, R. S. Al-Hasnawy, R. I. Jasim, N. F. Habubi, S. S. Chiad, Journal of Green Engineering, 10(9), 7018-7028 (2020); https://doi.org/10.1088/1742-6596/1999/1/012063
[28] S. S. Chiad, H. A. Noor, O. M. Abdulmunem, N. F. Habubi, M. Jadan, J. S. Addasi, Journal of Ovonic Research, 16 (1), 35-40 (2020). https://doi.org/10.15251/JOR.2020.161.35
[29] H. T. Salloom, E. H. Hadi, N. F. Habubi, S. S. Chiad, M. Jadan, J. S. Addasi, Digest Journal of Nanomaterials and Biostructures, 15 (4), 189-1195 (2020); https://doi.org/10.15251/DJNB.2020.154.1189
[30] R. S Ali, N. A. H. Al Aaraji, E. H. Hadi, N. F. Habubi, S. S. Chiad, Journal of Nanostructuresthis link is disabled, 10(4), 810–816 (2020); https://doi: 10.22052/jns.2020.04.014
[31] F. A. Jasima , Z. S. A. Mosa, N. F. Habubi, Y. H. Kadhim, S. S. Chiad, Digest Journal of Nanomaterials and Biostructures, 18 (3), 1039–1049 (2023); https://doi.org/10.15251/DJNB.2023.183.1039
[32] S. K. Muhammad, N. D. M. Taqi, S. S. Chiad, K. H. Abass, N. F. Habubi, Journal of Green Engineering, 11(2), 1287-1299 (2021).
[33] A. A. Abdul Razaq, F. H. Jasim, S. S. Chiad F. A. Jasim, Z. S. A. Mosa , Y. H. Kadhimd, Journal of Ovonic Research, 20 (2), 131 – 141 (2024); https://doi.org/10.15251/JOR.2024.202.131
[34] E. S. Hassan, D. M. Khudhair, S. K. Muhammad, A. M. Jabbar, M.O. Dawood, N. F. Habubi, S. S. Chiad, Journal of Physics: Conference Series ,1660 (1) 1660 012066 (2020); https://doi.org/10.1088/1742-6596/1660/1/012066
[35] A. S. Al Rawas, M. Y. Slewa, B. A. Bader, N. F. Habubi, S. S. Chiad, Journal of Green Engineering,10 (9), 7141-7153 (2020); https://doi.org/10.1021/acsami.1c00304
[36] R. S. Ali, H. S. Rasheed, N. F. Habubi, S.S. Chiad, Chalcogenide Letters,, 20 (1), 63–72 (2023; https://doi.org/10.15251/CL.2023.201.63
[37] A. Ghazai, K. Qader, N. F. Hbubi, S. S. Chiad, O. Abdulmunem, IOP Conference Series: Materials Science and Engineering, 870 (1), 012027 (2020);

https://doi.org/ 10.1088/1757-899X/870/1/012027
[38] R. S. Ali, M. K. Mohammed, A. A. Khadayeir, Z. M. Abood, N. F. Habubi and S. S. Chiad, Journal of Physics: Conference Series, 1664 (1), 012016 (2020); https://doi:10.1088/1742-6596/1664/1/012016
[39] A. A. Khadayeir, R. I. Jasim, S. H. Jumaah, N. F, Habubi, S. S. Chiad, Journal of Physics: Conference Series,1664 (1) (2020); https://doi.org/10.1088/1742-6596/1664/1/012009
[40] O. M. Abdulmunem, A. M. Jabbar, S. K. Muhammad, M. O. Dawood, S. S. Chiad, N. F. Habubi, Journal of Physics: Conference Series,1660 (1), 012055 (2020); https://doi.org/ 10.1088/1742-6596/1660/1/012055
[41] E. H. Hadi, M. A. Abbsa, A. A. Khadayeir, Z. M. Abood, N. F. Habubi, and S.S. Chiad, Journal of Physics: Conference Series, 1664 (1), 012069 (2020); https://doi.org/ 10.1088/1742-6596/1664/1/012069
[42] J. Li et al., Energy Storage Materials, 27, 187 (2020); https://doi.org/10.1016/j.ensm.2020.01.011
[43] K. Feng et al., Angew Chem Int Ed Engl, 55(39), 11950 (2016); https://doi.org/10.1002/anie.201604021
[44] S. S Chiad,, A. S. Alkelaby, K. S. Sharba,, Journal of Global Pharma Technology, 11 (7), 662-665, (2020); https://doi.org/10.1021/acscatal.1c01666
[45] Chiad, S.S., Noor, H.A., Abdulmunem, O.M., Habubi, N.F., Journal of Physics: Conference Series 1362(1), 012115 (2019); https://doi.org/10.1088/1742-6596/1362/1/012115
[46] B. A. Bader, S. K. Muhammad, A. M. Jabbar, K. H. Abass, S. S. Chiad, N. F. Habubi, J. Nanostruct, 10(4): 744-750, (2020); https://doi.org/ 10.22052/JNS.2020.04.007
[47] F. H. Jasim, H. R. Shakir, S. S. Chiad,N. F. Habubi, Y. H. Kadhi,, Jadan, M., Digest Journal of Nanomaterials and Biostructures, 18(4), 1385–1393 (2023); https://doi.org/10.15251/DJNB.2023.184.1385
[48] H. T. Salloom, R. I. Jasim, N. F. Habubi, S. S. Chiad, M. Jadan, J. S. Addasi, Chinese Physics B, 30 (6), 068505 (2021); https://doi.org/10.1088/1674-1056/abd2a7
[49] E. Onat et al., Journal of the Australian Ceramic Society, 57 (5), 1389 (2021); https://doi.org/10.1007/s41779-021-00643-9
[50] K. Y. Qader, R. A. Ghazi, A. M. Jabbar, K. H. Abass, S. S. Chiad, Journal of Green Engineering, 10 (10), 7387-7398 (2020); https://doi.org/10.1016/j.jece.2020.104011
[51] R. I. Jasim, E. H. Hadi, S. S. Chiad, N. F. Habubi, M. Jadan, J. S. Addasi, Journal of Ovonic Research, 19 (2), 187 – 196 (2023)..
[52] K. Y. Qader, E. H. Hadi, N. F. Habubi, S. S. Chiad, M. Jadan, J. S. Addasi, International Journal of Thin Films Science and Technology, 10 (1), 41-44 (2021); https://doi.org/ 10.18576/ijtfst/100107
[53] N. N. Jandow, M. S. Othman, N. F.Habubi, S. S. Chiad, K. A. Mishjil, I. A. Al-Baidhany, Materials Research Express, 6 (11), (2020); https://doi.org/10.1088/2053-1591/ab4af8
[54] M. D. Sakhil, Z. M. Shaban, K. S. Sharba, N. F. Habub, K. H. Abass, S. S. Chiad, A. S. Alkelaby, NeuroQuantology, 18 (5), 56-61 (2020); https://doi.org/10.14704/nq.2020.18.5.NQ20168
[55] E. S. Hassan, K. Y. Qader, E. H. Hadi, S. S. Chiad, N. F. Habubi, K. H. Abass, Nano Biomedicine and Engineering, 12(3), pp. 205-213 (2020); https://doi.org/10.5101/nbe.v12i3.p205-213
[56] M. S. Othman, K. A. Mishjil, H. G. Rashid, S. S. Chiad, N. F. Habubi, I. A. Al-Baidhany, Journal of Materials Science: Materials in Electronics, 31(11), 9037-9043 (2020); https://doi.org/10.1007/s10854-020-03437-0
[57] E. H. Hadi, D. A. Sabur, S. S. Chiad, N. F. Habubi, K., Abass, Journal of Green Engineering, 10 (10), 8390-8400 (2020); https://doi.org/10.1063/5.0095169
[58] M. S. İzgi et al. International Journal of Hydrogen Energy, 45 (60), 34857 (2020); https://doi.org/10.1016/j.ijhydene.2020.04.034
[59] K. S. Sharba, A. S. Alkelaby, M. D. Sakhil, K. H. Abass, N. F. Habubi, S. S. Chiad, Enhancement of urbach energy and dispersion parameters of polyvinyl alcohol with Kaolin additive, NeuroQuantology, 18 (3), 66-73 (2020);

https://doi.org/10.14704/NQ.2020.18.3.NQ20152
[60] A. A. Khadayeir, E. S. Hassan, S. S. Chiad, N. F. Habubi, K. H. Abass, M. H. Rahid, T. H. Mubarak, M. O. Dawod, I. A. Al-Baidhany, Journal of Physics: Conference Series 1234 (1), 012014, (2019); https://doi.10.88/1742-6596/1234/1/012014
[61] Hassan, E.S., Mubarak, T.H., Chiad, S.S., Habubi, N.F., Khadayeir, A.A., Dawood, M.O., Al-Baidhany, I. A. , Journal of Physics: Conference Series, 1294(2), 022008 (2019); https://doi.10.88/1742-6596/1294/2/022008
[62] M.O. Dawood, S.S. Chiad, A.J. Ghazai, N.F. Habubi, O.M. Abdulmunem, AIP Conference Proceedings 2213, 020102,(2020); https://doi.org/10.1063/5.0000136
[63] H. Ç. Kazıcı et al., Journal of Electronic Materials, 51 (5), 2356 (2022); https://doi.org/10.1007/s11664-022-09491-0
[64] E. Onat et al., Journal of the Australian Ceramic Society, 57 (5), 1389 (2021); https://doi.org/10.1007/s41779-021-00643-9